Effects of fine particles on terminal velocities of single bubbles in a narrow channel between parallel flat plates

Hashida, Masaaki

Hayashi, Kosuke

Tomiyama, Akio

(Citation)
International Journal of Multiphase Flow,127:103270

(Issue Date)
2020-06

(Resource Type)
journal article

(Version)
Accepted Manuscript

Effects of fine particles on terminal velocities of single bubbles in a narrow channel between parallel flat plates

Masaaki Hashida [a], Kosuke Hayashi [a], Akio Tomiyama [a, b]

[a] *Graduate School of Engineering, Kobe University, 1-1 Rokkodai, Nada, Kobe, Japan*

[b] *Corresponding author:* tomiyama@mech.kobe-u.ac.jp, TEL/FAX:*+81-78-803-6131*

Abstract

Effects of the presence of solid particles on the terminal velocities, V_B, of single bubbles in a narrow channel were investigated. The gap thickness of the narrow channel was 3 mm. The bubble diameter, d_B, was varied from 7 to 20 mm. Air, purified water and fine silica particles of 4.1 μm diameter were used for the gas, liquid and solid phases, respectively. The volume concentration of the particles, C_S, was from 0.20 to 0.40. The apparent slurry viscosity, μ_{SL}, ranged from 1.7 to 3.1 mPa·s. The applicability of a velocity correlation proposed for bubbles in gas-liquid systems to bubbles in slurry was examined. The following conclusions were obtained under the present experimental conditions: (1) the dependence of V_B on d_B in slurry is similar to that in glycerol-water solutions, and the bubble Reynolds number in slurry and a glycerol-water solution of the same Morton

number are almost the same for $C_S \leq 0.35$, and (2) the velocity correlation for gas-liquid systems is applicable to slurry with fine particles for $C_S \leq 0.35$ by using μ_{SL} instead of the liquid viscosity in the correlation.

Keywords

planar bubble, slurry, apparent viscosity, bubble lateral motion

1. Introduction

Bubbles in confined channel geometries are utilized in various practical systems (Akita and Yoshida, 1973; Bessler and Littman, 1987; Bush and Eames, 1998; Krishna et al., 2000; Yamanoi and Kageyama, 2010; Piedra et al., 2015; Wang et al., 2016). The shape and the motion of a bubble in a confined channel are affected by channel walls. Bubbles in a narrow channel between parallel flat plates, for instance, become planar and can only move along the channel walls. It is important to understand the bubble dynamics in such cases in designing and operating some practical systems.

Roig et al. (2012) measured the velocities, V_B, of air bubbles in stagnant water filled in a narrow channel of the gap thickness δ = 1 mm for a wide range of the Archimedes number, Ar, to investigate the bubble dynamics in detail. They observed that a bubble of

small Ar rose in a zigzagging path with periodic vortex shedding, whereas a large Ar bubble took a rectilinear path with unsteady vortices attaching to the bubble. They also found that the bubble Reynolds number, Re, was proportional to Ar. Filella et al. (2015) carried out experiments on bubbles in a narrow channel of δ = 3.1 mm and proposed an empirical correlation of Re in terms of Ar and δ/d_B to account for the effects of δ on V_B. Wang et al. (2016) pointed out that the gap thickness plays an important role in the bubble dynamics in a narrow channel, and they investigated the effects of δ and the bubble diameter, d_B, on V_B and reported that the ratio, δ/d_B, is required to correlate V_B for various δ. These correlations do not account for the viscous effect though the effects of the liquid viscosity on V_B would often be non-negligible in practical systems. In our previous study (Hashida et al., 2019), we measured V_B in a narrow channel filled with glycerol-water solutions to investigate the effects of the liquid viscosity on V_B and found that a change in the bubble path from zigzagging to rectilinear causes an abrupt change in V_B and proposed a V_B correlation by taking into account the viscous effect.

Tomiyama et al. (1996) measured terminal velocities of single air bubbles in stagnant water in narrow channels to evaluate air tightness criterion of unlined caverns for liquid petroleum gas (LPG) storage. They developed a velocity model for bubbles in liquids, which accounts for the effects of d_B and δ on V_B. Although an actual channel, i.e. cracks

of a rock around a LPG tank, may include particulate matter like sands (Miyanaga et al., 1994), their model does not account for the presence of particles. In waste water treatment processes, flat sheet membranes have often been used (Zhang et al., 2009; Drews et al., 2010; Böhm et al., 2014). In this case, suspended solids (SS) in sludge affect the motion of bubbles rising through narrow channels between membranes. Therefore understanding the effects of the presence of fine solid particles on the motion and V_B of bubbles in a narrow channel is important. Our knowledge on the particle effects on the bubble dynamics in a narrow channel is however still insufficient.

The terminal velocities of single bubbles in a narrow channel were measured in this study to investigate the effects of fine solid particles on the terminal velocity for a wide range of d_B ($7 \leq d_B \leq 20$ mm) and particle volumetric concentration, C_S ($0.20 \leq C_S \leq 0.40$).

2. Experimental

2.1 Experimental setup

Fig. 1 shows the experimental setup made of the two flat plates of transparent acrylic resin and the gas injection nozzle. The height, width and thickness between the plates were 620, 200 and 3.0 mm, respectively. The stainless nozzle for injecting single bubbles was located at the bottom of the narrow channel. The inner diameter of the nozzle was

2.0 mm. The x and z are the horizontal and vertical coordinates, and their origin is set at the nozzle tip.

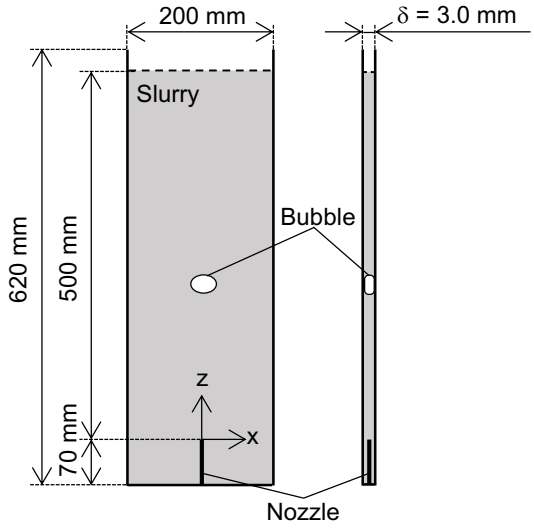

Fig. 1 Experimental setup

The channel was filled with slurry consisting of clean water and fine silica particles. Water purified by using a Millipore system (Elix 3) at room temperature (298±0.5 K) and atmospheric pressure was used for the liquid phase. Spherical hydrophilic porous silica particles (Fuji Silysia Chemical Ltd., SYLOSPHERE C-1504) and air were used for the solid and gas phases, respectively. The mean particle diameter, d_P, was 4.1 μm. The pore volume of the particles was 1.53×10^{-4} m^3/kg. The true density, ρ_T, and the apparent density, ρ_P, of the particles were 2250 kg/m^3 and 1270 kg/m^3, respectively. The ρ_P was

evaluated by taking the volume-weighted average of ρ_T and the density, ρ_L, of clean water filling the pores. The C_S tested were 0.20, 0.30, 0.35 and 0.40. The apparent densities, ρ_{SL}, and the apparent viscosities, μ_{SL}, of slurry at each C_S are summarized in **Table 1**, in which M is the Morton number defined by

$$M = \frac{\mu_{SL}^4 (\rho_{SL} - \rho_G) g}{\rho_{SL}^2 \sigma^3} \tag{1}$$

where σ is the surface tension (0.072 N/m), and g the magnitude of the acceleration of gravity. The gas density, ρ_G, and the gas viscosity were 1.2 kg/m^3 and 1.8 mPa·s, respectively. The ρ_L and the liquid viscosity, μ_L, were 997 kg/m^3 and 0.89 mPa·s, respectively. The densities, the viscosities and σ were measured by using a densimeter (Ando Keiki Co., Ltd., JIS B7525), a viscometer (A&D Co., Ltd., SV-10) and a pendant bubble method (Lin et al., 1990; Pan et al., 1998), respectively. Uncertainties in ρ_{SL}, μ_{SL} and σ estimated at 95% confidence were 0.02%, 4.2% and 3.3%, respectively. Orvalho et al. (2018) measured σ of slurry consisting of water and silica particles (d_P = 100 μm) and confirmed that σ is the same as that of clean water, implying that the particles do not bring any surfactants into water. Hence the systems used in the present experiments were clean.

Table 1 Physical properties of slurry (298±0.5 K)

C_S	μ_{SL} [mPa·s]	ρ_{SL} [kg/m^3]	log$M$
0.20	1.7	1051	–9.7
0.30	2.3	1077	–9.2
0.35	2.7	1092	–8.9
0.40	3.1	1105	–8.7

The ρ_{SL} was also measured using the densimeter and was compared with the following equation as shown in **Fig. 2**:

$$\rho_{SL} = \rho_P C_S + \rho_L (1 - C_S) \tag{2}$$

Good agreement between the data and Eq. (2) confirms the validity of ρ_P.

Fig. 3 shows measured μ_{SL}. The increase in C_S increases μ_{SL} and μ_{SL} at C_S = 0.40 is about three times larger than μ_L. The following correlation proposed by Toda and Furuse (2006) gives good evaluations for the present data:

$$\frac{\mu_{SL}}{\mu_L} = \frac{1 - 0.5 C_S}{(1 - C_S)^3} \tag{3}$$

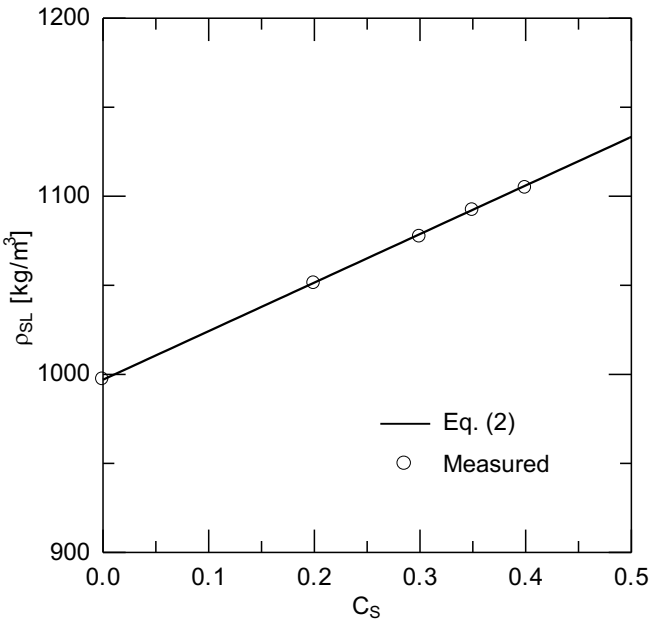

Fig. 2 Comparison between Eq. (2) and measured ρ_{SL}

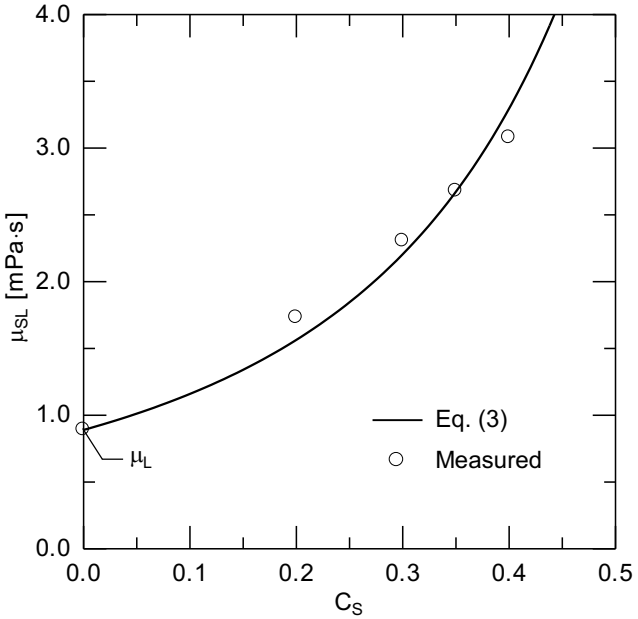

Fig. 3 Comparison between Eq. (3) and measured μ_{SL}

Sedimentation velocities of silica particles, V_S, were estimated based on the Stokes law.

The V_S was negligibly small compared with bubble velocities, i.e. $V_S \sim 1.0 \times 10^{-5}$ m/s.

Experiments on bubbles in glycerol-water solutions were also carried out for comparison with the data of slurry. The glycerol concentration, C_{GL}, of the glycerol-water solutions were 0.28 and 0.33. The data for C_{GL} = 0.21 and 0.38 obtained in Hashida et al. (2019) will also be used in the following sections. The fluid properties of the glycerol-water solutions are shown in **Table 2**, in which M were calculated using μ_L and ρ_L instead of μ_{SL} and ρ_{SL}. The fluid properties of the glycerol-water solutions are almost the same as the apparent fluid properties of the slurry given in **Table 1**.

Table 2 Physical properties of glycerol-water solutions (298±0.5 K)

C_{GL}	μ_L [mPa·s]	ρ_L [kg/m^3]	σ [N/m]	log$M$
0.21	1.7	1047	0.071	−9.6
0.28	2.3	1063	0.071	−9.2
0.33	2.7	1077	0.071	−8.8
0.38	3.1	1087	0.069	−8.6

2.2 Measurement method

The terminal velocity and the diameter of a single bubble were measured by processing bubble images. Successive images were taken by using a high-speed video camera (Photron Ltd., FASTCAM SA-X2) and a fluorescent light source was used for back

illumination. **Fig. 4(a)** shows an example of bubbles. The spatial and temporal resolutions were 0.20 mm/pixel and 1/125 s, respectively. The projected area, $A(z)$, of a bubble and the instantaneous rise velocity, $V(z)$, were measured by using an image processing method consisting of binarization and edge detection algorithms (Hosokawa and Tomiyama, 2003) (**Fig. 4(b)**). The bubble diameter, $d(z)$, was calculated as

$$d(z) = \sqrt{\frac{4A(z)}{\pi}} \tag{4}$$

The d_B was evaluated by averaging $d(z)$ for $300 \leq z \leq 400$ mm. The uncertainty in d_B estimated at 95% confidence was less than 2%. The experimental range of d_B was from 7 to 20 mm. The geometric center, $x_g(z)$, of a bubble was also obtained (**Fig. 4(c)**). The $V(z)$ was calculated from the moving distance in the z direction during the time duration between two successive images. **Fig. 5** shows $V(z)$ of a small bubble (d_B = 7.0 mm) and a large bubble (d_B = 19.0 mm) at C_S = 0.30. Small bubbles periodically fluctuated, and therefore, V_B were obtained by averaging $V(z)$ for three periods of oscillation. On the other hand, $V(z)$ of large bubbles were almost constant. The V_B of large bubbles were obtained by averaging $V(z)$ for $300 \leq z \leq 400$ mm. We confirmed that the bubbles reached the terminal conditions at $z \leq 300$ mm.

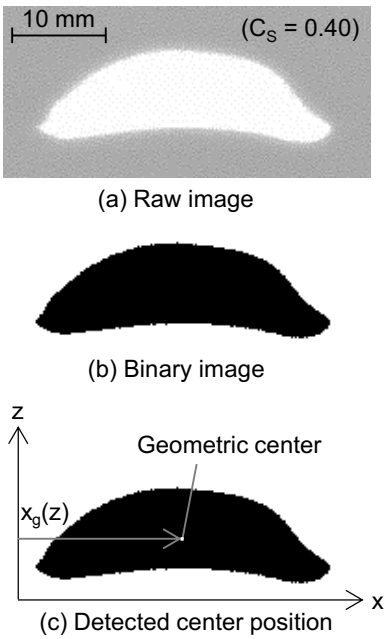

Fig. 4 Image processing for measurements of A and geometric center, $x_g(z)$, of bubble at d_B = 16.2 mm and C_S = 0.40

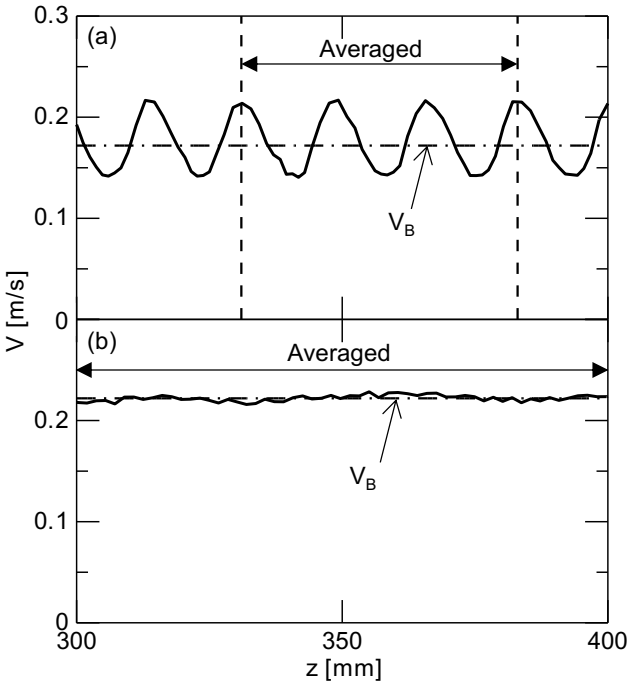

Fig. 5 Instantaneous rise velocities and V_B at (a) d_B = 7.0 and (b) 19.0 mm (C_S = 0.30)

Fig. 6 shows a bubble with zigzagging motion and the path of the geometric center (dotted line). The mean path (solid line), (x_c, z_c), of the center of a bubble was represented as a linear function,

$$x_c = az_c + b \tag{5}$$

by using the least square fit, where a and b are constants. The $\phi(z)$ in the figure is the distance between the mean path and the geometric center calculated by

$$\phi(z) = \frac{\left| az - x_g(z) + b \right|}{\sqrt{a^2 + 1}} \tag{6}$$

The standard deviation, s, from the mean path was calculated by

$$s = \sqrt{\frac{1}{z_2 - z_1} \int_{z_1}^{z_2} \phi(z)^2 \, dz} \tag{7}$$

where z_1 and z_2 are 300 and 400 mm, respectively. The s will be used as an indicator of the amplitude of the bubble lateral motion in the following section.

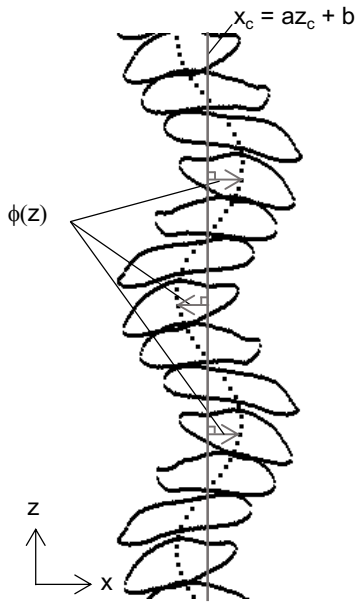

Fig. 6 Bubble path at d_B = 9.5 mm and C_S = 0.40 (log$M$ = –8.7 and Re_{SE} = 385, where Re_{SE} is the bubble Reynolds number defined by Eq. (8))

3. Results and discussion

3.1 Bubble shape, path and terminal velocity

Bubble shapes at each slurry concentration are shown in **Fig. 7**. The bubble shapes at d_B = 7.0 mm ((a), (f) and (k)) are distorted ellipsoidal and their paths (dotted line) are zigzag. Comparing (a) and (b) shows that the amplitude of the path oscillation increases with increasing d_B, and the shape deformation also becomes larger. However the amplitude of the path oscillation at d_B = 11.4 mm ((c)) is much smaller than that of (b) at 11.1 mm in spite of the small difference in d_B. This abrupt change in the bubble motion from zigzagging to rectilinear can also be observed at the other C_S ((g)-(h) and (l)-(m)).

The bubble shapes and paths of larger bubbles are spherical-cap like and almost rectilinear. The d_B for the transition from zigzagging to rectilinear decreases with increasing C_S, in other words, with increasing μ_{SL} ((c), (h) and (m); d_B for the path transition decreases from 11.4 to 9.9 mm). Just before the path transition ((b), (g) and (l)), the bubble shapes are elongated in the lateral direction and are similar although d_B in each case are different (d_B = 11.1 ~ 9.7 mm from C_S = 0.20 to 0.40). After the path transition ((c), (h) and (m)), the bubble shapes are similar for $C_S \leq 0.30$. However, the bubble motion and the shape at C_S = 0.40 are different from the others. The bubble shape at C_S = 0.40 has the left-right symmetry and the amplitude of the bubble lateral motion is very small. The larger bubbles in the rectilinear path regime at C_S = 0.40 ((n) and (o)) are also more stable and symmetric than those at lower C_S ((d), (e), (i) and (j)).

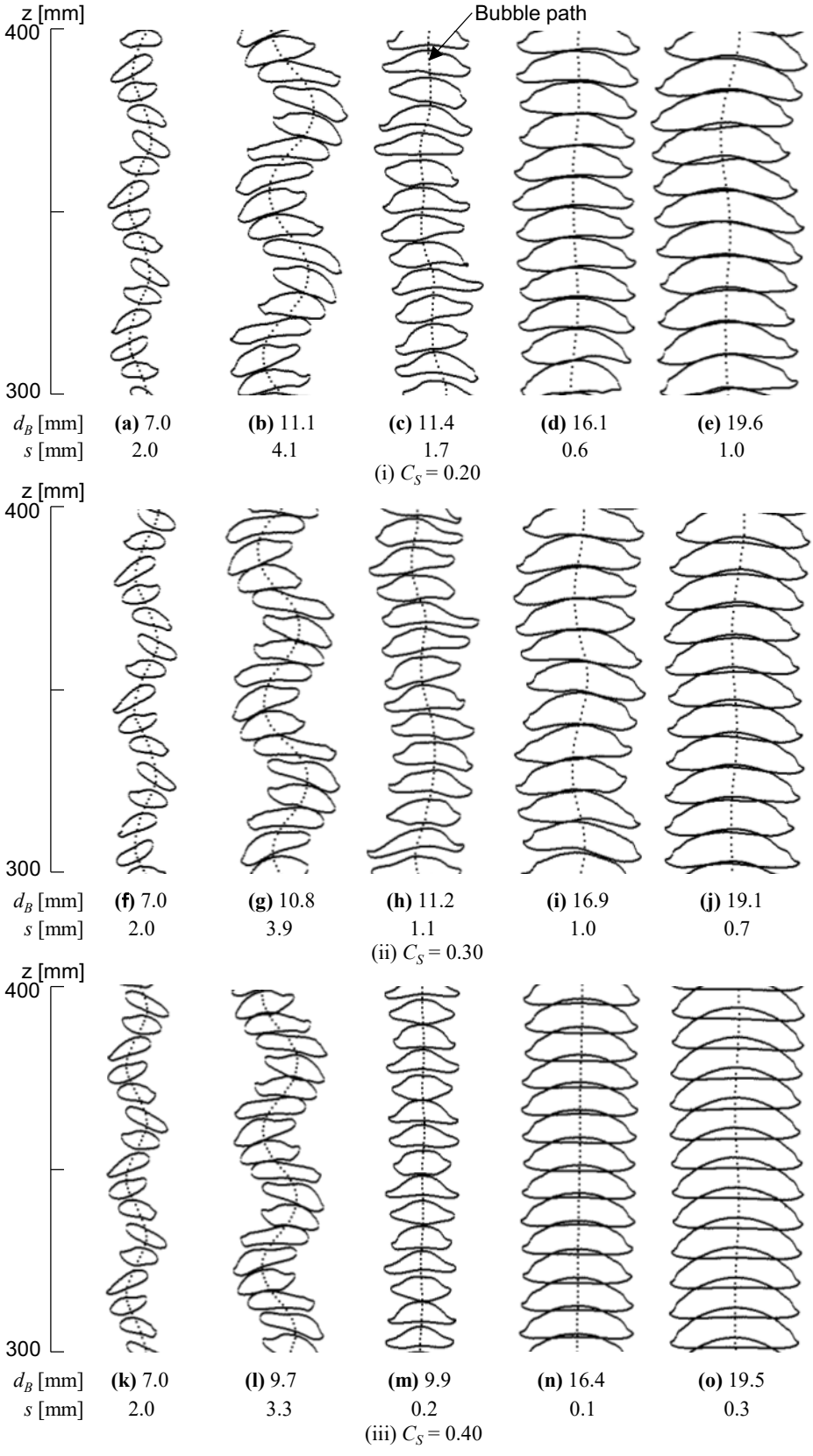

Fig. 7 Bubble shapes and paths (time duration between two consecutive images is 40 ms.)

Fig. 8 shows s of bubbles. In all C_S conditions, s increases with increasing d_B up to a certain d_B, and then, s abruptly decreases. We reported in our previous study (Hashida et al., 2019) that d_B for the abrupt decrease in s becomes smaller as μ_L increases. Therefore μ_{SL} plays a similar role as μ_L in the transition of bubble motion from zigzagging to rectilinear. Discussion on the bubble path transition in terms of dimensionless groups is given in Appendix A.

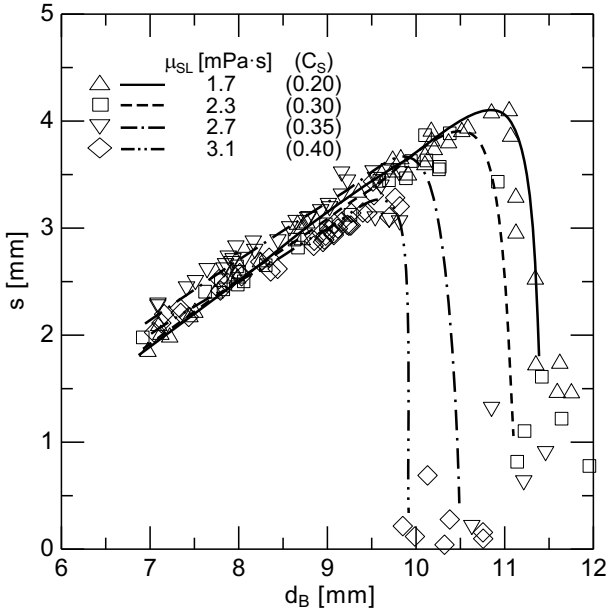

Fig. 8 s of bubbles

Fig. 9 shows V_B of bubbles in the slurry. At C_S = 0.30, V_B of bubbles with zigzagging motion increases with increasing d_B up to d_B ~ 8.0 mm (Regime 1), whereas for 8.0 < d_B ≤ 10.9 mm V_B decreases with increasing d_B. Then V_B abruptly increases at d_B ~ 11.2 mm.

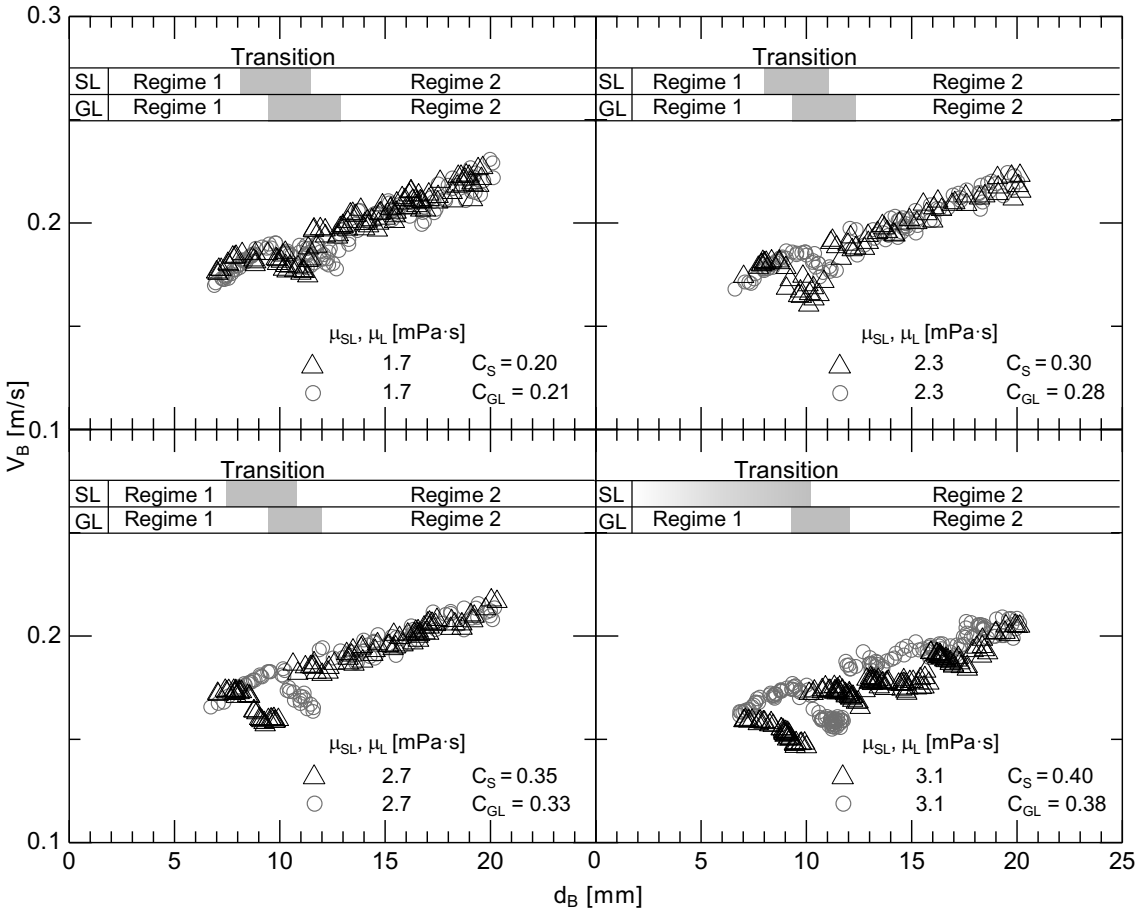

Fig.9 Comparisons of V_B between bubbles in slurry and glycerol-water solutions (SL and GL denote slurry and glycerol-water solution, respectively, and gray region represents transition regime)

This d_B corresponds to that for the path transition (transition regime). For d_B > 11.2 mm, V_B of bubbles with rectilinear path again increases with increasing d_B (Regime 2). This complex trend is the same for C_S = 0.20 and 0.35 and also found for bubbles in the glycerol-water solutions, for which we pointed out in Hashida et al. (2019) that V_B strongly relates with the bubble lateral motion, i.e. due to the use of the potential energy for the lateral motion, V_B of bubbles with zigzagging motion are lower than those with

rectilinear motion. The V_B of bubbles in the slurry are compared with those in the glycerol-water solutions in **Fig. 9**. The comparisons clearly show that, up to C_S = 0.35, V_B of Regime 1 and 2 in the slurry are almost the same as those in the glycerol-water solutions of the same M. The range of d_B for the transition regime in the slurry however slightly differ from that in the glycerol-water solution. The difference in the d_B range of path transition increases with increasing C_S, resulting in the increase in the difference in V_B between the slurry and the glycerol-water solution in the transition regime with increasing C_S. This implies that the complex trend of V_B in the transition regime cannot be described by the apparent fluid properties only. The V_B at C_S = 0.40 largely differs from that at C_{GL} = 0.38 not only in the transition regime but also in Regime 2 even at the same M. Note that no bubbles were classified into Regime 1 in the present d_B range at C_S = 0.40. The V_B data in **Fig. 9** are replotted on the Re_{SE}–Eo_{SE} plane in Appendix B, where Eo_{SE} is the Eötvös number.

The shapes of bubbles in slurry are compared with those in the glycerol-water solutions in **Fig. 10**. In each condition of C_S and C_{GL}, the small bubbles on the left side are in Regime 1 and the large bubbles on the right side are in Regime 2. At d_B ~ 7.0 mm, the bubbles in slurry are slightly wider than those in the glycerol-water solutions. The bubble shapes in slurry and the glycerol-water solutions are similar in Regime 2 for $C_S \leq 0.35$,

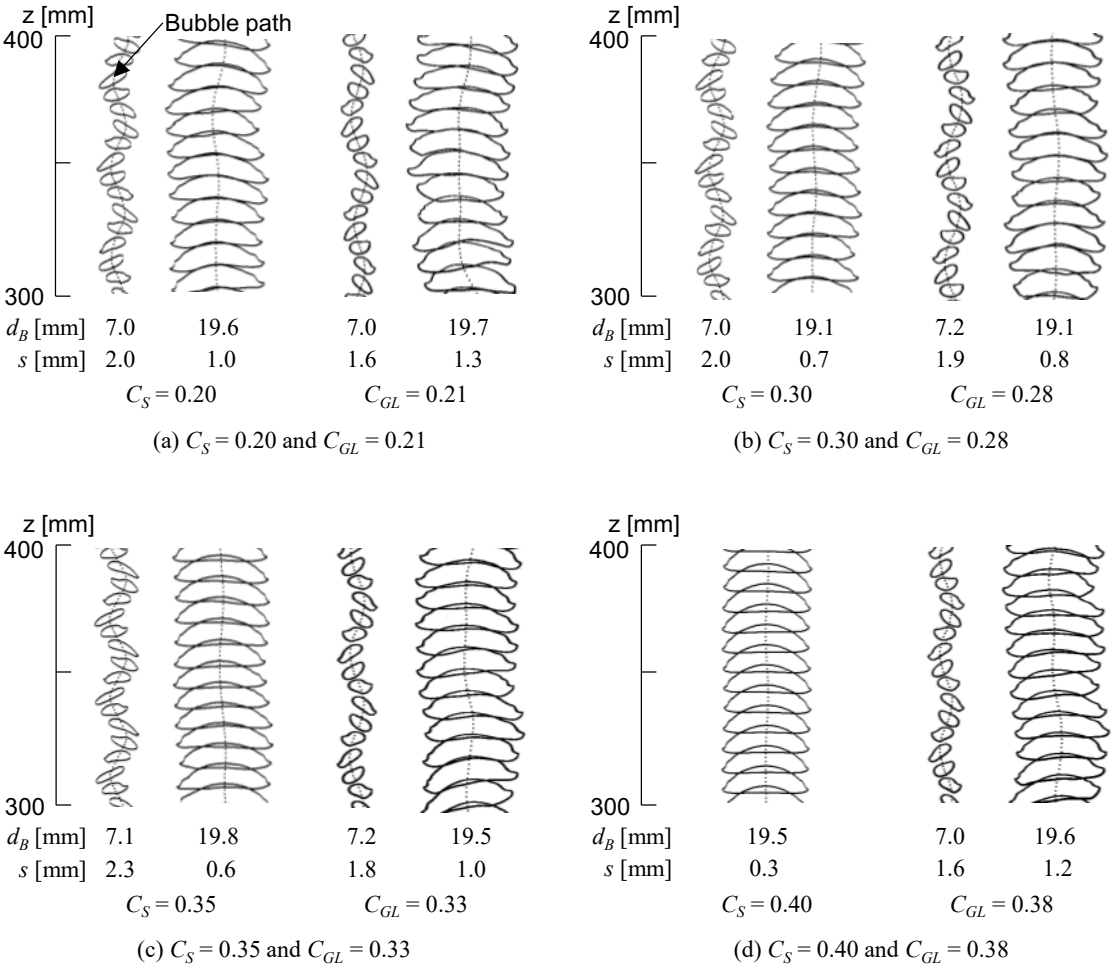

Fig. 10 Bubble shapes and paths in Regime 1 and 2 for $C_S \leq 0.40$ and $C_{GL} \leq 0.38$

while the bubble shape at $C_S = 0.40$ is more stable than that at $C_{GL} = 0.38$.

The dependence of V_B on d_B at $C_S = 0.40$ is complicated. The V_B and s at $C_S = 0.40$ and V_B at $C_{GL} = 0.38$ are shown in **Fig. 11**. The data at $C_S = 0.40$ have several abrupt changes in V_B represented by the labels of A, B and C while there is no remarkable change of V_B at $C_{GL} = 0.38$ except for the first V_B jump, which was caused by the transition from

zigzagging to rectilinear motion (Hashida et al., 2019). The abrupt changes in V_B at C_S = 0.40 take place at d_B ~ 9.9, 12.8 and 15.9 mm. The second V_B jump occurs at d_B ~ 12.8 mm where s abruptly increases. The widths, W, and the heights, H, of bubbles were evaluated by averaging instantaneous bubble width and height as shown in **Fig. 12**, and the relations between them and d_B are shown in **Fig. 13**. The W for $9.9 < d_B < 12.8$ mm increases with increasing d_B while H is almost constant. The W slightly decreases at d_B ~ 9.9 mm (dotted line A) when the abrupt transition of the bubble motion occurs. Then, the abrupt decrease in W and the increase in H take place at d_B ~ 12.8 mm (B). Before the second V_B jump (**Fig. 14(a)**), the bubble path is rectilinear and the bubble shows fluttering, whereas after the V_B jump (**Fig. 14(b)**) the bubble path fluctuates and the flutter is mitigated. The fluctuation of bubble path abruptly mitigates at d_B ~ 15.9 mm (C) (**Figs. 14(c)** and **(d)**) accompanying with the decrease in W, which resulted in the third V_B jump. On the other hand, there are no remarkable changes in the trends of W and H at C_{GL} = 0.38 as shown in **Fig. 13**.

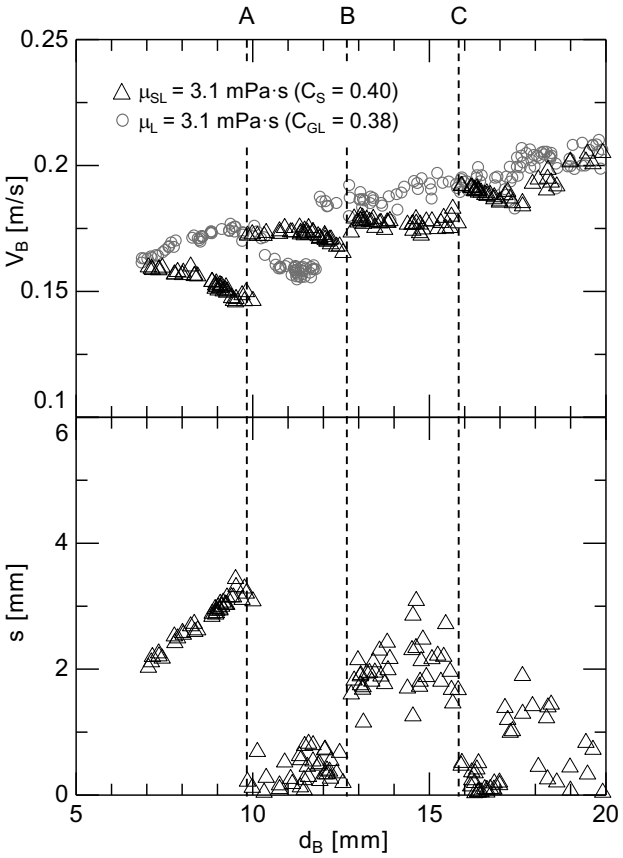

Fig. 11 V_B and s of bubbles at C_S = 0.40 and V_B at C_{GL} = 0.38

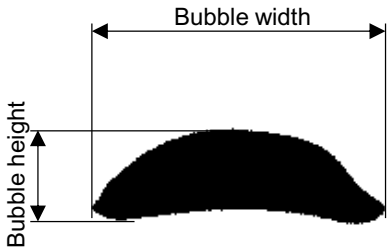

Fig. 12 Definitions of bubble width, W, and height, H

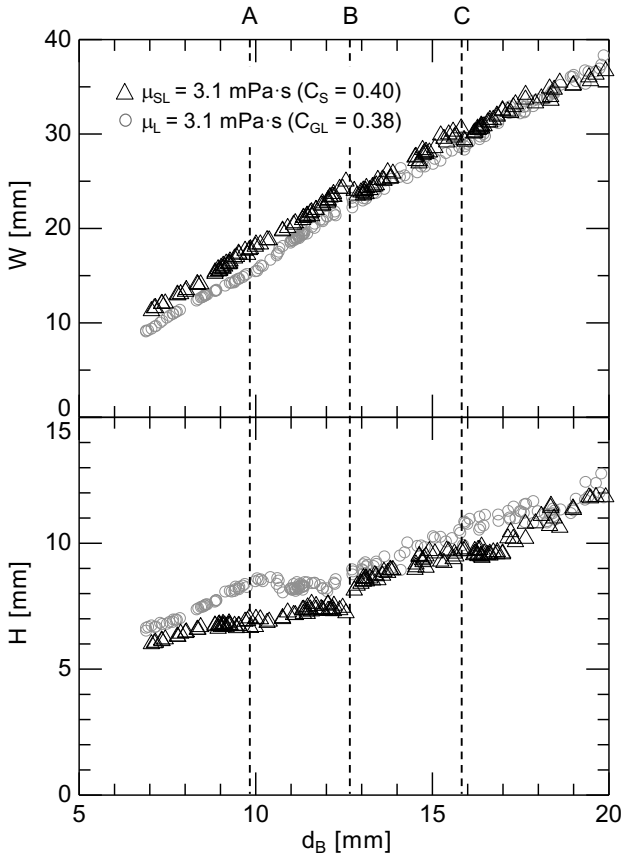

Fig. 13 W and H at $C_S = 0.40$ and $C_{GL} = 0.38$

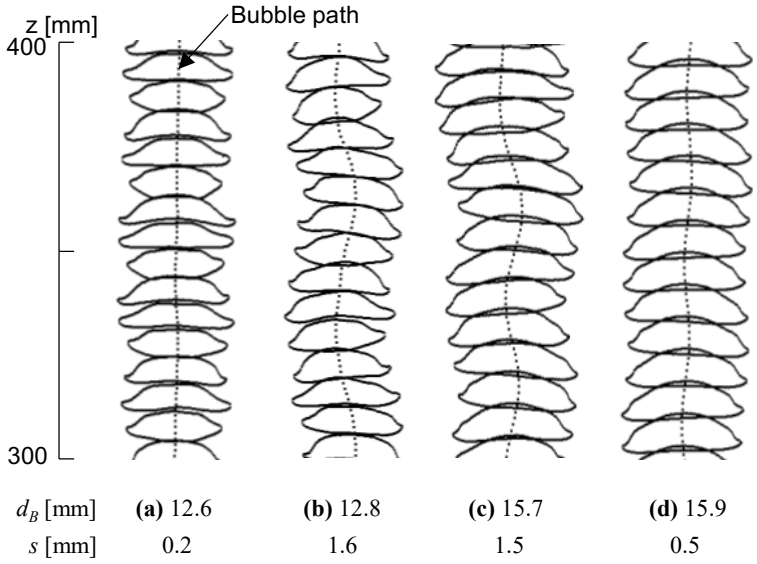

Fig. 14 Bubble shapes and paths at $C_S = 0.40$

Fig. 15 shows the bubble Reynolds number, Re_{SE}, plotted against the Archimedes number, Ar_{SE}, defined by

$$Re_{SE} = \frac{\rho_{SL} V_B d_{SE}}{\mu_{SL}} \tag{8}$$

$$Ar_{SE} = \frac{\sqrt{\rho_{SL}(\rho_{SL} - \rho_G) g d_{SE}^3}}{\mu_{SL}} \tag{9}$$

where d_{SE} is the sphere-volume-equivalent bubble diameter ($d_{SE} = [3d_B^2\delta/2]^{1/3}$) and ρ_{SL} and μ_{SL} are replaced with ρ_L and μ_L, respectively, in the glycerol-water solution cases. The Re_{SE} of the slurry are proportional to Ar_{SE}. The slurry data represented in terms of the dimensionless groups agree with those of the glycerol-water solutions. Hence Re_{SE} in slurry and a glycerol-water solution of the same M are almost the same.

We proposed the following bubble Reynolds number correlation for bubbles in glycerol-water solutions (Hashida et al., 2019):

$$Re_{SE} = 1.13\sqrt{f(M)}\, Ar_{SE} \tag{10}$$

The function, $f(M)$, of the Morton number ($M = \mu_L^4 \Delta\rho g/\rho_L^2\sigma^3$) is given by

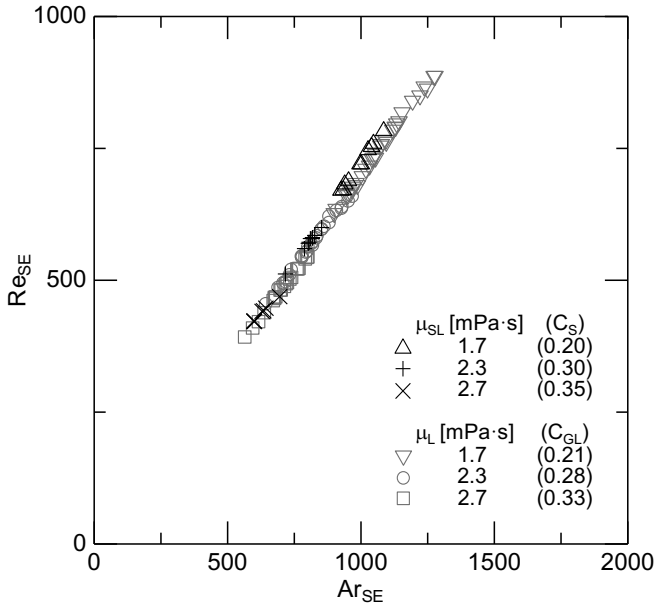

(a) Regime 1

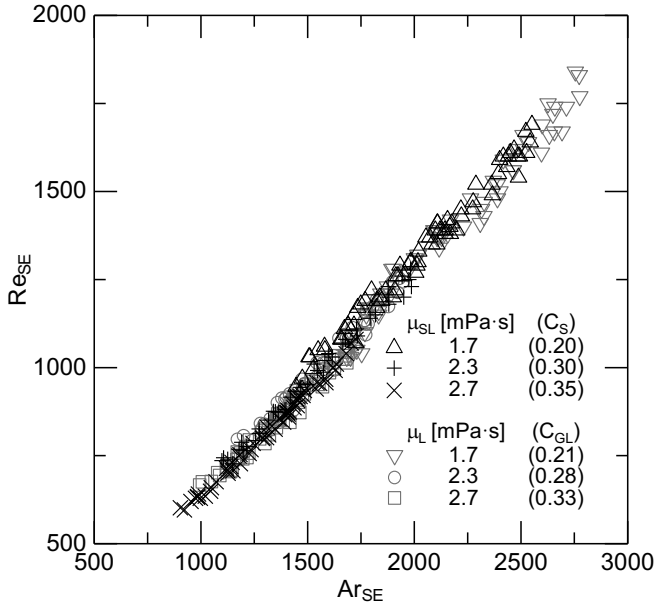

(b) Regime 2

Fig. 15 Re_{SE} plotted Ar_{SE} for $C_S \leq 0.35$ and $C_{GL} \leq 0.33$

$$f(M)=\begin{cases}\left(C_1+C_2\tanh(C_3\log(M)+C_{R1})\right)^{C_4} & \text{for Regime1}\\ \left(C_1+C_2\tanh(C_3\log(M))\right)^{C_4} & \text{for Regime2}\end{cases} \tag{11}$$

where $C_1 = 0.824$, $C_2 = 0.146$, $C_3 = -0.168$, $C_4 = 27$ and $C_{R1} = 0.33$. The coefficients were determined by fitting the functional form to the data of $C_{GL} = 0$ (clean water), 0.21, 0.38, 0.67 and 0.83. We added the present data of $C_{GL} = 0.28$ and 0.33 into the database of V_B in glycerol-water solutions and reconsidered the functional form of Eq. (11), resulted in

$$f(M)=\begin{cases}\left(C_1+C_2\tanh(C_3\log(M)+C_4)\right)^{C_5}+C_{R1} & \text{for Regime1}\\ \left(C_1+C_2\tanh(C_3\log(M)+C_4)\right)^{C_5} & \text{for Regime2}\end{cases} \tag{12}$$

where $C_1 = 0.791$, $C_2 = 0.109$, $C_3 = -0.303$, $C_4 = -1.52$, $C_5 = 9.47$ and $C_{R1} = 0.056$. Eq. (10) can be rewritten as

$$V_B = 1.21\sqrt{f(M)}\left(\frac{\delta}{d_B}\right)^{\frac{1}{6}}\sqrt{\frac{(\rho_L-\rho_G)gd_B}{\rho_L}} \tag{13}$$

The V_B in the slurry were evaluated using Eq. (13), while the liquid physical properties were evaluated using the apparent physical properties of slurry. The calculated V_B are compared with the data for $C_S \leq 0.35$ and $C_{GL} \leq 0.33$ in **Fig. 16**. Eq. (13) gives good

evaluations not only for bubbles in the glycerol-water solutions but also for those in slurry. **Fig. 17** shows the comparison between Eq. (13) and the measured data at C_S = 0.20, 0.30 and 0.35 except for the transition regime, and all the data in Regime 1 and 95 % of the data in Regime 2 are to within ±5% errors. Therefore Eq. (13) is also applicable to bubbles in the slurry at least for $C_S \leq 0.35$ and d_P = 4.1 μm. Comparisons between the present data and the correlation, Eq. (10), in the dimensionless form are given in Appendix C.

4. Conclusion

The terminal velocities, V_B, of single bubbles in a narrow channel filled with slurry were measured to investigate the effects of the presence of fine particles on V_B. The gap of the narrow channel was 3 mm. The bubble diameter was varied from 7 to 20 mm. Air and purified water were used for the gas and liquid phases, respectively. The spherical silica particles of 4.1 μm diameter was used for the solid phase. The volume concentration of the particles, C_S, was varied from 0.20 to 0.40. The applicability of a velocity correlation proposed for gas-liquid systems to bubbles in slurry was examined. The conclusions obtained under the present experimental conditions are as follows:

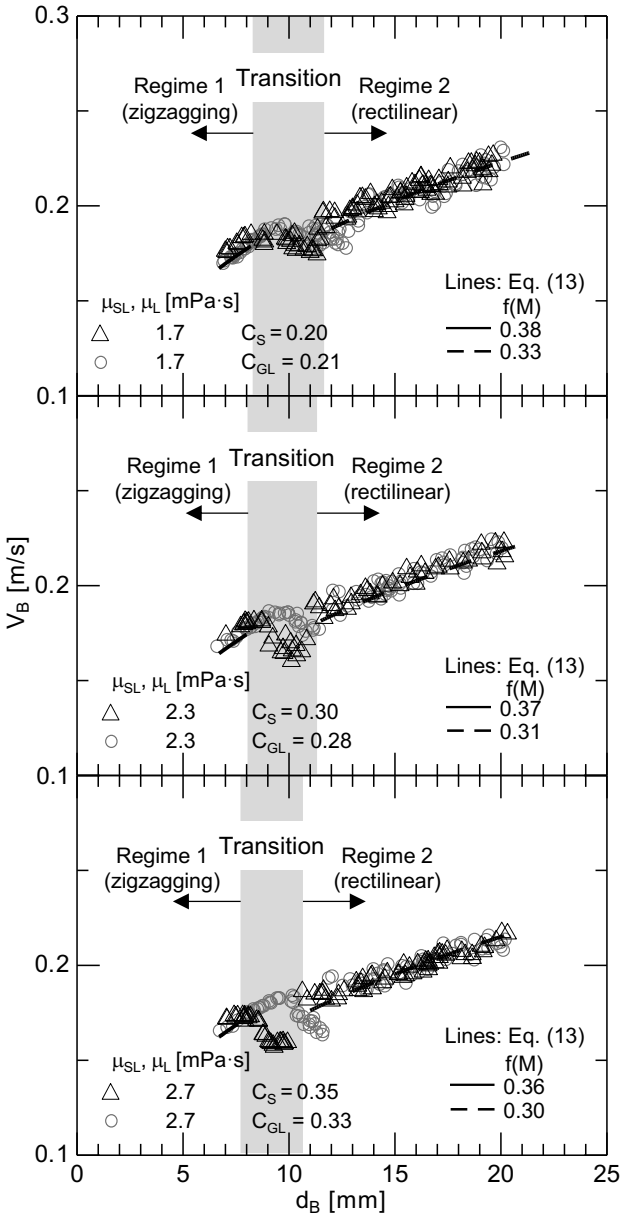

Fig. 16 V_B data for $C_S \leq 0.35$ and Eq. (13) with Eq. (12)

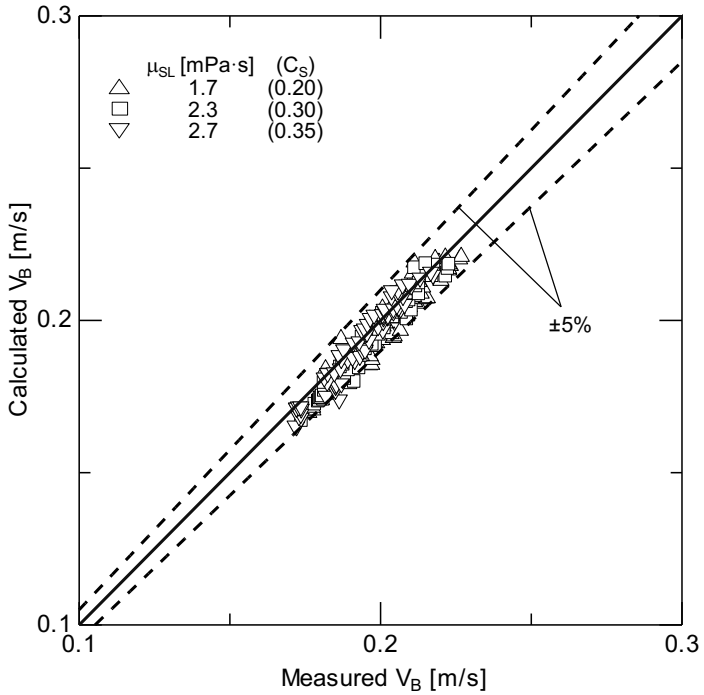

Fig. 17 Comparison between measured and calculated V_B

(1) The bubble motion in slurry abruptly transits from zigzagging to rectilinear at a certain critical bubble diameter. The increase in the apparent viscosity decreases the critical diameter, i.e. the effect of the apparent viscosity on the critical diameter is similar to that of the liquid viscosity.

(2) The dependence of V_B on the bubble diameter in slurry is similar to that in glycerol-water solutions, and the bubble Reynolds number in slurry and a glycerol-water solution having the same Morton number are almost the same for $C_S \leq 0.35$ except

for the transition regime. Therefore the effect of the presence of fine particles on V_B is the same as that of the liquid viscosity in the zigzagging and rectilinear path regimes.

(3) The velocity correlation for gas-liquid systems is applicable to slurry with fine particles for $C_S \leq 0.35$ by using the apparent viscosity instead of the liquid viscosity in the correlation.

(4) The dependence of V_B on the bubble diameter at $C_S = 0.40$ is more complicated than that in the glycerol-water solution, implying that the effects of fine particles on the bubble motion at the high C_S cannot be described by the apparent fluid properties only.

Acknowledgement

The authors would like to express their thanks to the financial support by JSPS KAKENHI Grant Number 18H03756.

Appendix

A. Discussion on bubble motion in terms of dimensionless groups

The s is normalized by the critical bubble diameter, d_C, at the beginning of Regime 2 (the rectilinear path regime) in **Fig. A1**, where the horizontal axis is Re_{SE}. The different curves for the different C_S mean that the path transition cannot be described in terms of Re_{SE} only, and the critical bubble Reynolds number, Re_{SE}^C, for the path transition depends on M, where d_C and Re_{SE}^C are summarized in **Table A1**. On the other hand, the maximum value of s/d_C less depends on M, i.e. $s/d_C \sim 0.34$ just before the abrupt decrease in s/d_C. Bubbles in Regime 1 oscillate and are accompanied with vortex shedding in their wakes due to hydrodynamic instability, and s/d_C increases with increasing Re_{SE} since the potential energy used for the lateral motion increases. However, when the wake becomes large enough, vortices behind a bubble attach to the bubble rear (Roig et al., 2012) and consequently the bubble motion becomes stable with a rectilinear path. Although the wake structure was not observed in the present experiments, it may start to change from the periodic vortex shedding mode to the attaching vortex mode when s/d_C reaches the upper limit, $s/d_C \sim 0.34$.

Fig. A2 shows Re_{SE}^C plotted against M. The data of $M = 1.7 \times 10^{-11}$ were obtained from our previous paper (Hashida et al., 2019). The Re_{SE}^C can be simply expressed as a function

of M:

$$Re_{SE}^{C} = 1.55M^{-0.289} \tag{A1}$$

The Re_{SE}^{C} of bubbles in glycerol-water solutions (Hashida et al., 2019) are also shown in the figure. The Re_{SE}^{C} in slurry are somewhat smaller than those in the glycerol-water solutions, and therefore, the effects of fine particles on the bubble motion cannot be fully explained in terms of the apparent viscosity only.

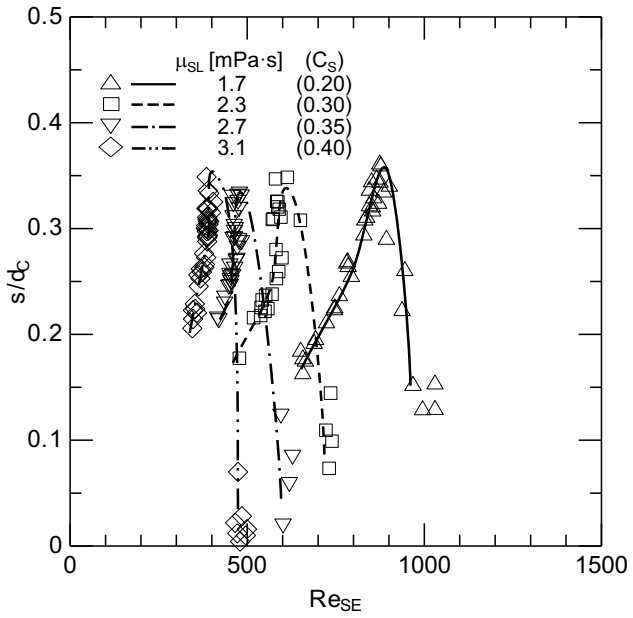

Fig. A1 s/d_C plotted against Re_{SE}

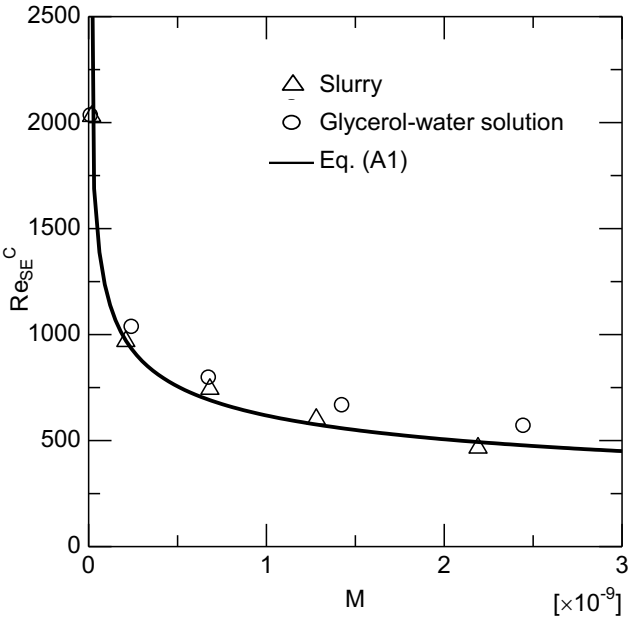

Fig. A2 Re_{SE}^{C} plotted against M

Table A1 d_C and Re_{SE}^{C}

C_S	0	0.20	0.30	0.35	0.40
d_C [mm]	13.0	11.4	11.2	10.6	9.9
Re_{SE}^{C}	2030	968	742	601	466

B. Relation between bubble Reynolds number and Eötvös number

The relation between Re_{SE} and the Eötvös number, Eo_{SE} (= $[\rho_{SL}-\rho_G]gd_{SE}^2/\sigma$), is shown in **Fig. B1**, in which the gray region represents the transition regime. In Regime 1 Re_{SE} increases with increasing Eo_{SE}. The behavior of Re_{SE} is complicated in the transition regime. Then Re_{SE} again increases with increasing Eo_{SE} in Regime 2. The abrupt increase in Re_{SE} can also be seen at the end of the transition regime as on the V_B–d_B plane in **Fig. 9**. The data, $Re_{SE}(Eo_{SE})$, depend on M, and therefore, $Re_{SE} = f(Eo_{SE}, M)$. It should however

be noted that Re_{SE} can also be expressed as $Re_{SE}(Ar_{SE}, M)$ since $Eo_{SE} = [Ar_{SE}^4 M]^{1/3}$. The correlation, Eq. (10), uses the latter form.

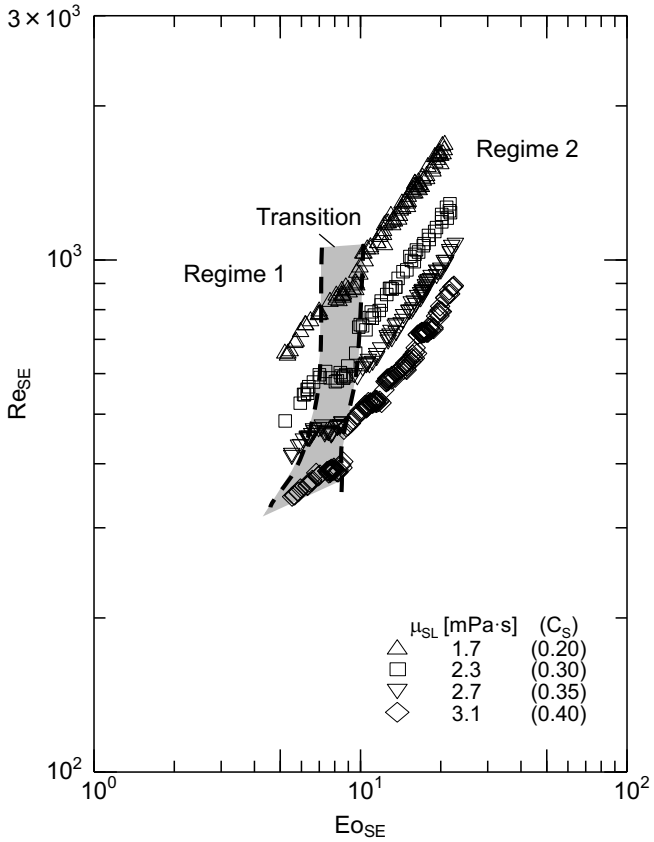

Fig. B1 Re_{SE} plotted against Eo_{SE}

C. Comparisons between empirical correlation in dimensionless form and experimental data

Fig. C1 shows comparisons between Eq. (10) and the data on the Re_{SE}–Ar_{SE} plane. The good agreement clearly shows the validity of Eq. (10) for the slurry systems even though it is for gas-liquid systems in the absence of fine particles.

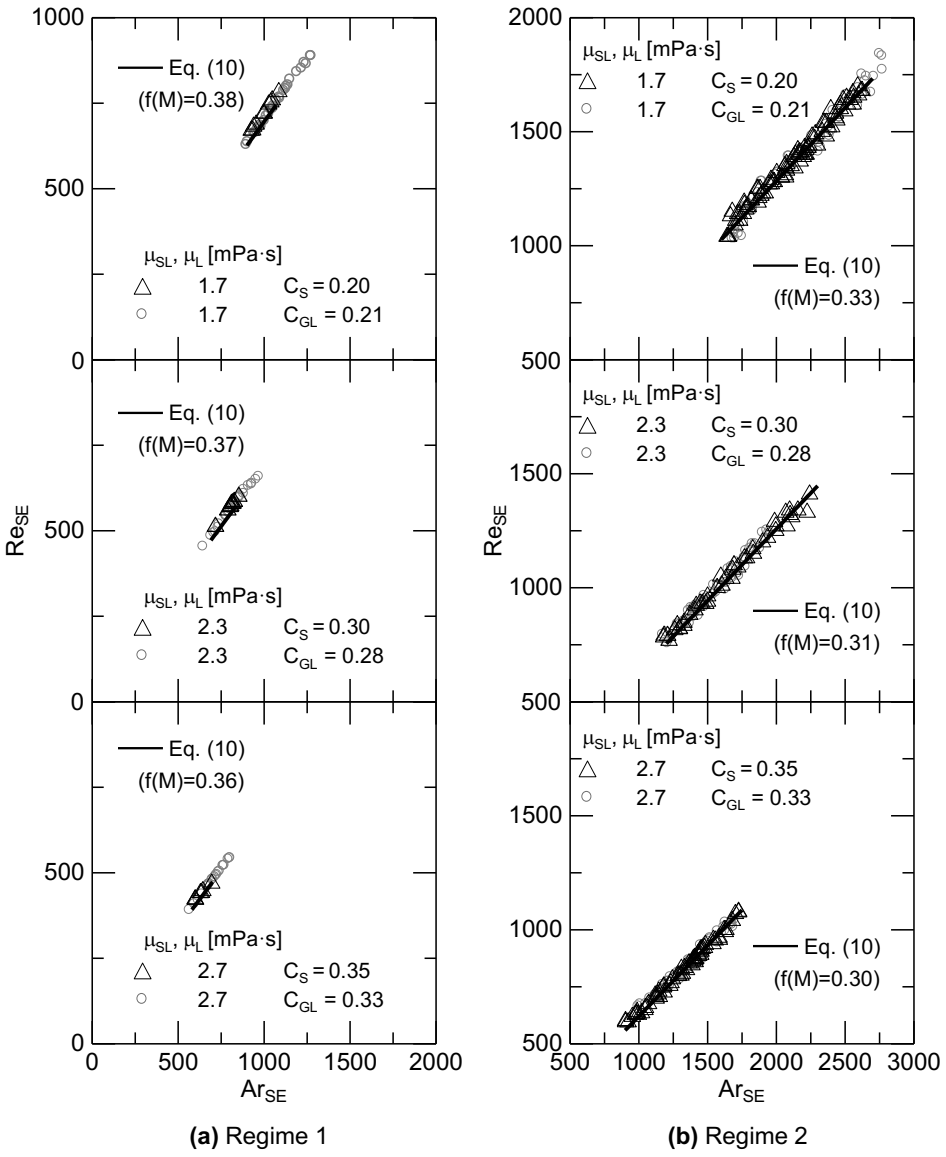

(a) Regime 1 **(b)** Regime 2

Fig. C1 Comparisons between Eq. (10) and present data

References

Akita, K., Yoshida, F., 1973. Gas holdup and volumetric mass transfer coefficient in bubble columns. Ind. Eng. Chem. Process Des. Dev. 12, 76–80.

Bessler, W.F., Littman, H., 1987. Experimental studies of wakes behind circularly capped bubbles. J. Fluid. Mech. 185, 137–151.

Böhm, L., Kurita, T., Kimura, K., Kraume, M., 2014. Rising behaviour of single bubbles in narrow rectangular channels in Newtonian and non-Newtonian liquids. Int. J. Multiph. Flow 65, 11–23.

Bush, J.W.M., Eames, I., 1998. Fluid displacement by high Reynolds number bubble motion in a thin gap. Int. J. Multiph. Flow. 24, 411–430.

Drews, A., Prieske, H., Meyer, E.-L., Senger, G., Kraume, M., 2010. Advantageous and detrimental effects of air sparging in membrane filtration: Bubble movement, exerted shear and particle classification. Desalination 250, 1083–1086.

Filella, A., Ern, P., Roig, V., 2015. Oscillatory motion and wake of a bubble rising in a thin-gap cell. J. Fluid Mech. 778, 60–88.

Hashida, M., Hayashi, K., Tomiyama, A., 2019. Rise velocities of single bubbles in a narrow channel between parallel flat plates. Int. J. Multiph. Flow 111, 285–293.

Hosokawa, S., Tomiyama, A., 2003. Lateral force acting on a deformed single bubble due to the presence of wall. Trans. Jpn. Soc. Mech. Eng., Ser. B, 69, 2214–2220 in Japanese.

Krishna, R., Baten, J.M., Urseanu, M.I., Ellenberger, J., 2000. Rise velocity of single circular-cap bubbles in two-dimensional beds of powders and liquids. Chem. Eng. Processing 39, 433–440.

Lin, S.Y., Mckeigue, K., Maldarelli, C., 1990. Diffusion-controlled surfactant adsorption studied by pendant drop digitization. AIChE J. 36, 1785–1795.

Miyanaga, Y., Makita, T., Ebara, M., Hatano, T., 1994. A non-rpessurised grouting method using clay for controlling groundwater –a theory of clay grouting and the construction record of Kuji underground oil storage plant–. J. Jpn. Soc. Eng. Geology 35, 23–35 in Japanese.

Orvalho, S., Hashida, M., Zednikova, M., Stanovsky, P., Ruzicka, M.C., Sasaki, S., Tomiyama, A., 2018. Flow regimes in slurry bubble column: Effect of column height and particle concentration. Chem. Eng. J. 351, 799–815.

Pan, R., Green, J., Maldarelli, C., 1998. Theory and experiment on the measurement of kinetic rate constants for surfactant exchange at an air/water interface. J. Colloid Interface Sci. 205, 213–230.

Piedra, S., Ramos, E., Herrera, J.R., 2015. Dynamics of two-dimensional bubbles. Phys. Rev. E 91, 063013.

Roig, V., Roudet, M., Risso, F., Billet, A.M., 2012. Dynamics of a high-Reynolds-number bubble rising within a thin gap. J. Fluid Mech. 707, 444–466.

Toda, K., Furuse, H., 2006. Extension of Einstein's viscosity equation to that for concentrated dispersions of solutes and particles. J. Biosci. Bioeng. 102, 524–528.

Tomiyama, A., Hosokawa, S., Ebara, M., Miyanaga, Y., Kawakubo, Y., Kinoto, H., 1996. Terminal velocity and drag coefficient of single air bubbles in stagnant water filling in narrow parallel walls. Japanese J. Multiph. Flow 10, 146–153 in Japanese.

Wang, X., Klaasen, B., Degrève, J., Mahulkar, A., Heynderickx, G., Reyniers, M.F., Blanpain, B., Verhaeghe, F., 2016. Volume-of-fluid simulations of bubble dynamics in a vertical Hele-Shaw cell. Phys. Fluids 28, 1–13.

Yamanoi, I., Kageyama, K., 2010. Evaluation of bubble flow properties between flat sheet membranes in membrane bioreactor. J. Membr. Sci. 360, 102–108.

Zhang, K., Cui, Z., Field, R.W., 2009. Effect of bubble size and frequency on mass transfer in flat sheet MBR. J. Membr. Sci. 332, 30–37.